November 2002

ELSEVIER

Materials Letters 56 (2002) 838–841

MATERIALS LETTERS

www.elsevier.com/locate/matlet

Synthesis of thick $Ni_{66}Cr_5Mo_4Zr_6P_{15}B_4$ amorphous alloy coating and large glass-forming ability by laser cladding

X. Wu [a,*], B. Xu [b], Y. Hong [a]

[a] State Key Lab of Nonlinear Mechanics, Institute of Mechanics, Chinese Academy of Sciences, Beijing 100080, PR China
[b] College of Materials Science and Engineering, Taiyuan University of Technology, Taiyuan 030024, PR China

Received 16 November 2001; accepted 21 November 2001

Abstract

A thick amorphous alloy (*a*-alloy) coating was synthesized by laser cladding. The *a*-alloy had a multicomponent chemistry, i.e., $Ni_{66}Cr_5Mo_4Zr_6P_{15}B_4$ (in atom%). The maximum thickness of the coating is 0.8 mm. The *a*-alloy coating had large glass-forming ability (GFA) with wide supercooled liquid region (SLR) ranging from 52 to 61 K through the coating. The reason for high GFA in the *a*-alloy coating was discussed.

Keywords: Amorphous alloy coating; Glass-forming ability; Laser cladding

1. Introduction

Novel bulk amorphous alloys (*a*-alloys) of multicomponent chemistry, distinct from conventional *a*-alloys, have demonstrated highly dense, randomly packed structures and large glass-forming ability (GFA) through strong resistance to crystallization in the supercooled liquid region (SLR) [1–3]. Zr-, Mg-, La-, Pd-, Ti-, and Fe-based bulk *a*-alloys have been developed using various methods, e.g., water quenching, arc melting, copper mold casting, high-pressure die casting, and unidirectional solidification, etc. The long substantial interest has arisen for synthesis of *a*-alloy coatings for unusual improvements of the surface-related properties and high-energy laser processing is a promising technique [4–7]. The generation of *a*-alloy coatings was, however, limited to a large extent, due to the fact that the laser synthesis of conventional *a*-alloy layers requires the ultra-high cooling rate often above 10^5 K/s and the resulting thickness is limited to the magnitude of several tens of microns. In the present letter, we have synthesized a thick multicomponent Ni-based *a*-alloy coating by laser cladding and investigated the reason for large GFA.

2. Experimental details

The substrate was AISI 1045 steel, with the composition of 0.43C, 0.21Si, 0.35Mn, balance Fe (in wt.%). Specimens were $80 \times 40 \times 30$ mm^3 in dimension.

The coating alloy was a multicomponent powder mixture with a nominal composition $Ni_{66}Cr_5$-

* Corresponding author. Chemical Engineering Department, Visiting Research Association, Cleveland State University, 1960 E24th St., SH 455, Cleveland, OH 44115, USA. Tel.: +1-216-523-7280; fax: +1-216-687-9220.
E-mail address: x.l.wu@csuohio.edu (X. Wu).

0167-577X/02/$ - see front matter © 2002 Elsevier Science B.V. All rights reserved.
PII: S0167-577X(02)00624-9

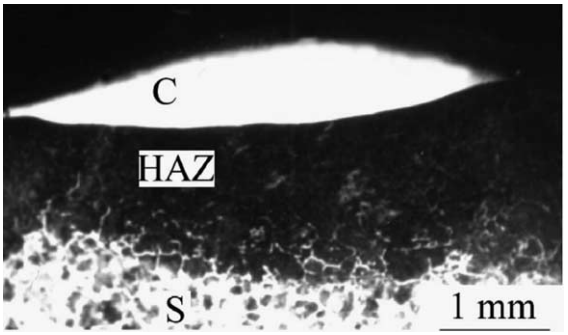

Fig. 1. Optical micrograph showing the transverse of the coating. (C: coating, HAZ: heat-affected zone, S: substrate).

$Mo_4Zr_6P_{15}B_4$ (in at.%). The pure metals, pre-alloyed Ni–P alloy and pure crystal B powders ranged from 25 to 44 μm in size and from 99.9 to 99.995 wt.% in purity, respectively. Mixed evenly for 10 h in an argon gas atmosphere, powders were pasted on the surface of samples using acetone with a thickness of 0.8 mm.

A 10-kW cw CO_2 laser was used to produce the coating. Here, the laser surface cladding technique was adopted. The laser cladding consisted of melting the substrate surface with pre-coated Ni-based alloy powders, allowing them to solidify rapidly, and then forming a coating with its structure, chemistry, and property different from those of the substrate. The process had only a little volumetric dilution ratio. Selection of the range of values for the independent process parameters, i.e., laser power, beam size, and beam scanning speed, was based on the order of magnitude of power density and appropriate interaction time. Resultantly, the laser was operated at power of 7.5 kW and process speed of 40 mm/s. The specimen was in a shielding box supplied with high-purity argon.

The coating was identified by optical microscope, X-ray diffractometry (XRD), and transmission electron microscope (TEM). The thermal stability associated with glass transition, supercooled liquid, and crystallization was examined at a heating rate of 0.17 K/s by differential scanning calorimetry (DSC). The melting temperature (T_m) was also measured by differential thermal analysis. All specimens for XRD, DSC, and TEM analyses were thin slices. Slices of 50 μm thick, parallel to the top surface of the substrate, were cut using a slow-speed cut-off saw. Thin TEM films of 3 mm in diameter were then dimpled and argon-ion-beam thinned to perforation at the room temperature. The shape of DSC films is 10×3 $mm^2 \times 50$ μm. Successive cuts assured inspection at a well-identified depth of the coating. The microhardness was also measured across the coating transverse with a Vickers hardness tester under a 200-g indentation load.

3. Results

Fig. 1 is an optical morphology showing the transverse of the coating (C), heat-affected zone (HAZ), and substrate (S), respectively. Note that the coating has a maximum thickness of 0.8 mm.

Fig. 2 shows the XRD pattern at 0.3 mm deep from the top surface of the coating. Only a broad halo peak is seen and no diffraction peak corresponding to a crystalline phase is observed. Fig. 3 is an electron diffraction pattern (EDP) taken from the area of 2 μm in diameter at 0.25 mm deep from the top surface. The EDP consists of halo rings, typical of an *a*-alloy. A large number of XRD and TEM observations are made at various depths and the results remained the same. It is reasonably deduced that the crystal nucleation is suppressed and an *a*-alloy is produced in the coating.

Fig. 4 shows the DSC curve of the layer at 0.41 mm deep from the surface. Note that with an increase in temperature, the curve shows the amorphous transition, followed by the appearance of a wide super-

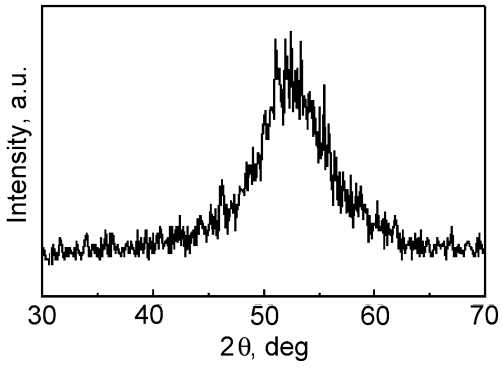

Fig. 2. XRD pattern of the *a*-alloy coating (0.3 mm deep from the top surface).

Fig. 3. Electron diffraction pattern of the *a*-alloy coating (0.25 mm deep from the top surface).

cooled liquid region (SLR) and crystallization. The glass transition temperature, T_g, corresponds to the temperature where the curvature of the endothermic reaction on the DSC curve is maximum and can be measured within an accuracy ± 2 K, while the onset temperature of crystallization, T_x, is defined as the temperature at which the tangential lines between the supercooled liquid and the exothermic peak intersect with each other. It is worthwhile to note that the temperature interval of the SLR, ΔT_x $(=T_x - T_g)$ value is as large as 55 K. In addition, the T_g/T_m value is 0.61. The large SLR implies a high thermal stability of the supercooled liquid against crystallization. There

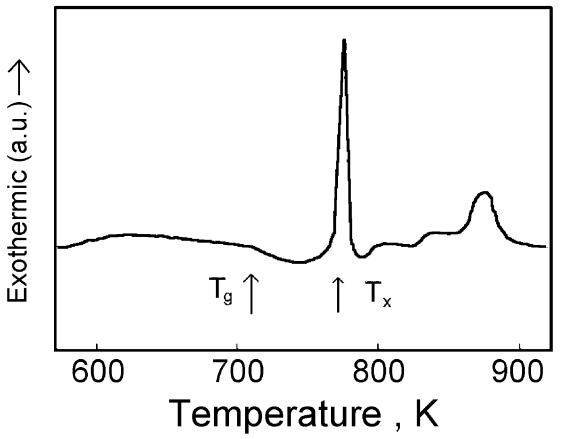

Fig. 4. DSC curve of the *a*-alloy coating (0.41 mm deep from the top surface).

Table 1
DSC results measured at different depths of the coating

D (mm)[a]	T_g (K)	T_x (K)	ΔT_x (K)	T_m (K)	T_g/T_m
0.18	722	783	61	1128	0.64
0.32	720	778	58	1143	0.63
0.41	719	774	55	1179	0.61
0.59	717	769	52	1195	0.60

[a] D: distance from the top surface of the coating.

is a clear tendency for the GFA to increase with increasing ΔT_x and T_g/T_m.

The variation of ΔT_x with depth is further examined, as shown in Table 1. Note that ΔT_x increases from 52 to 61 K upon approaching the top surface. Both T_g and T_x increase monotonously, but the degree of an increase in T_x is larger than that for T_g. Resultantly, the extension of ΔT_x is due to the increase in T_x that exceeds the degree of the increase in T_g. This result indicates clearly that the increase in ΔT_x is attributed to the retardation of crystallization.

Akatsuka et al. [8] obtained bulk *a*-alloys in the Ni–M–P (M = Ti, Zr, Hf, Nb) ternary systems with a large SLR of 49 K. The SLR increases to 64 K by simultaneous addition of Cr, Mo, and B elements to the Ni–Nb–B system [9]. Thus, ΔT_x values obtained in the present *a*-alloy coating are very similar to those of the above bulk Ni-based *a*-alloys.

The hardness of the *a*-alloy layer is shown in Fig. 5. The reported values are the averages of five measurements. Note that a gradient distribution of hardness presents, ranging from 952 to 1270 Hv.

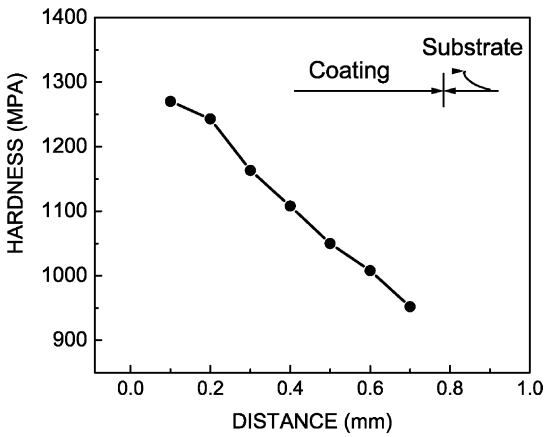

Fig. 5. Variation of microhardness with depth.

4. Discussion

The large GFA of the present *a*-alloys in the coating can be explained below. The base composition in the present coating is the Ni–Zr–P system, which satisfies the empirical rules for bulk *a*-alloy formation, i.e., (i) multicomponent alloy systems consisting more than three constituent elements, (ii) significantly different atomic size ratios above about 13%, and (iii) suitable negative heats of mixing among the constituent elements [3]. The addition of Cr, Mo, and B causes the sequential change in the atomic size in the order of Zr≫Mo>Cr>Ni>P≫B, as well as the generation of new atomic pairs with various negative heats of mixing. It was observed that the bulk Fe–Zr–B *a*-alloy with a large SLR has a unique linked structure in which the trigonal prisms consisting of Fe and B atoms are connected by Zr atoms and the formation of the linked structure increases the thermal stability of the supercooled liquid against crystallization [10]. Considering the similarity of the atomic size ratios and electronegativity in the alloy components, the present Ni-based alloy can be presumed to have a similar long-range linked structure. The long-range linked atomic configurations are also in a tightly bonding state and have difficulty with rearranging of the constituent elements, leading to the large SLR before crystallization through the suppression of nucleation and growth of the crystalline phase in the SLR by inhibiting the long distance diffusion and increasing the melting viscosity. B atoms with a much smaller atomic size relative to other constituents tighten the alloy structure and decrease the free volume, and play a crucial role in the formation of this kind of structure. This is supported by other experimental results [11]. The more close-packed structural characteristics of the *a*-alloy cause the high viscosity in the supercooled liquid state and make the redistribution of atoms on a large range scale in the melt extremely difficult. Meanwhile, the local atomic configuration of short-range order and composition in the conventional *a*-alloy resemble the corresponding equilibrium compound with a composition near that of the *a*-alloy. The crystallization process occurs easily because it does not need a long diffusion of atoms, so a high cooling rate is needed for suppressing nucleation and growth of the crystalline phase. The multicomponent *a*-alloy, however, has a highly random close-packed structure, and its composition and local structure are much different from those of the crystallization phase [1,3]. This structural feature requires that the component elements have to redistribute substantially. On the other hand, the highly random close-packed structure and the large viscosity make the redistribution of atoms on a large scale extremely difficult. In addition, the more components, the more difficult for all constituents to satisfy simultaneously the local structural and compositional requirements of the crystalline phase.

5. Conclusion

Thick Ni-based *a*-alloy coatings with nominal composition $Ni_{66}Cr_5Mo_4Zr_6P_{15}B_4$ have been synthesized by laser surface cladding. The maximum thickness of the coating is 0.8 mm. The *a*-alloy coating had excellent glass forming. The *a*-alloy coating also reveals high microhardness.

Acknowledgements

This research was supported by National Natural Science Foundation, National Outstanding Young Scientific Foundation of China, and The Chinese Academy of Sciences.

References

[1] W.L. Johnson, Mater. Sci. Forum 35 (1996) 225–227.
[2] A. Peker, W.L. Johnson, Appl. Phys. Lett. 63 (1993) 2342.
[3] A. Inoue, Mater. Trans., JIM 36 (1995) 866.
[4] C.J. Lin, F. Spaepen, Appl. Phys. Lett. 41 (8) (1992) 721–723.
[5] F. Hirose, M. Takagi, H. Mori, Y. Kitoh, T. Imura, Jpn. J. Appl. Phys. 31 (1992) 3940.
[6] X. Wu, Y. Hong, Metall. Mater. Trans. 31A (2000) 3123.
[7] X. Wu, Y. Hong, Surf. Coat. Technol. 141 (2001) 141.
[8] R. Akatsuka, T. Zhang, H. Koshiba, A. Inoue, Mater. Trans., JIM 40 (1999) 258.
[9] X. Wang, I. Yoshii, A. Inoue, Y. Kim, I. Kim, Mater. Trans., JIM 40 (1999) 1130.
[10] A. Inoue, T. Zhang, T. Itoi, A. Takeuchi, Mater. Trans., JIM 38 (1997) 359.
[11] W.H. Wang, Z.X. Bao, C.X. Liu, D.Q. Zhao, J. Eckert, Phys. Rev. B 61 (2000) 3166.